Numerical research of the compressible flow in a vortex tube using OpenFOAM software

Article *in* Thermal Science · January 2016

DOI: 10.2298/TSCI160223195B

3 authors, including:

Jela Burazer
Faculty of Mechanical Engineering
11 PUBLICATIONS **27** CITATIONS

NUMERICAL RESEARCH OF THE COMPRESSIBLE FLOW IN A VORTEX TUBE USING OPENFOAM SOFTWARE

by

Jela M. BURAZER, Aleksandar S. ĆOĆIĆ* and Milan R. LEČIĆ

Department of Fluid Mechanics, Faculty of Mechanical Engineering, University of Belgrade,

Belgrade, Serbia

Original scientific paper
DOI: 10.2298/TSCI????N (5 UDC)

The work presented in this paper is dealing with numerical simulation of energy separation mechanism and flow phenomena within a Ranque-Hilsch vortex tube. Simulation of turbulent, compressible, highly swirling flow inside vortex tube is performed using RANS approach, with Favre averaged conservation equations. For turbulence closure, $k-\varepsilon$ and $k-\omega$ SST models are used. It is assumed that the mean flow is axisymmetric, so the 2-D computational domain is used. Computations were performed using open-source CFD software OpenFOAM. All compressible solvers available within OpenFOAM were tested, and it was found that most of the solvers cannot predict energy separation. Code of two chosen solvers, which proved as the most robust, is modified in terms of mean energy equation implementation. Newly created solvers predict physically accepted behavior in vortex tube, with good agreement with experimental results. Comparison between performances of solvers is also presented.

Key words: *vortex tube, compressibility, OpenFOAM, energy separation.*

Introduction

A vortex tube is a simple device whose main operational principle is separation of high pressure flow into two regions with relatively low pressures and with temperatures higher and lower than the temperature of the inlet flow. This device has no moving parts. It consists of a simple tube with inlet section, where compressed gas flow enters the pipe tangentially through one or more nozzles, and two outlets for exiting cold and hot streams of gas. Due to high swirl, created at the inlet section, the flow splits into hot gas stream near the pipe wall, and cold gas stream which flows in opposite direction along the axis (core region). Vortex tube has many practical applications. Some of them are: cooling tools for diamonds grinding, cooling tools for metal cutting, cooling of vehicle cabins, robot controls, cooling of electrical and electronic control panels, food cooling, cooling of equipment in laboratories dealing with explosive chemicals and cooling of firemen's suits. It is also used for air-conditioning of aircraft cabins or its parts, air-conditioning of space rockets and space-crafts, as well as for individual air-conditioning, then in hyperbaric chambers, for particle separation, for separation of gas and liquid mixture, in nuclear reactors, etc.

This device is discovered by Ranque [1], demonstrating the effect of temperature separation of gases due to adiabatic expansion in core region and adiabatic compression of the flow near pipe wall. Hilsch [2] improved Ranque's results introducing internal friction

* Corresponding author; e-mail: acocic@mas.bg.ac.rs

between gas layers. These pioneering theoretical works on thermodynamic explanations of separation phenomenon have been later improved by numerous authors, for example by Kurosaka [3] and Ahlborn et al. [4], [5]. However, till today there is no complete theory which explains the phenomenon of energy separation in the vortex tube. During the past decade the research studies on vortex tube have been separated in two main groups: experimental works, which use experimental data for explanation of the phenomenon, and numerical and analytical work where the flow inside the tube is studied, with the goal to determine implications for temperature separation.

One of the first numerical computations of flow inside the vortex tube was done by Fröhlingsdorf and Unger in [6], who explored the mechanism of the energy separation phenomenon using of $k-\varepsilon$ model within the commercial CFX software. The model included effects of turbulence and compressibility and results agreed well with previous experimental work of other authors. In [6] it is claimed that the exchange of energy between cooled and heated fluid layers in the vortex tube can be explained as a consequence of mechanical work between these layers as they rotate at different circumferential speeds. Aljuwayhel et al. in [7] use two-equation $k-\varepsilon$ and RNG $k-\varepsilon$ models within commercial software FLUENT to simulate the flow inside vortex tube, using the assumption that the flow is axisymmetric. Their research shows that intensity of stratification of temperature field increases with increasing length of the vortex tube. However, they also find the existence of critical value of pipe length, after which the increase in length has no longer a positive effect on the operation of vortex tube. Authors also conclude that the RNG $k-\varepsilon$ turbulence model gives better results. Skye et al. [8] also use $k-\varepsilon$ and RNG $k-\varepsilon$ model for axisymmetric computations of the flow in different geometry of the vortex tube, but they obtain more accurate results with $k-\varepsilon$ model. Behera et al. [9] investigate both experimentally and numerically the influence of different shapes of nozzles, as well as their number, on the total energy separation inside the vortex tube. For numerical computations authors use commercial Star-CD software, with $k-\varepsilon$ and RNG $k-\varepsilon$ turbulence models. Eiamsa-ard and Promvonge [10] conducted a numerical analysis of the vortex tube performance using standard $k-\varepsilon$ and algebraic Reynolds stress model, using in-house code named TEFESS. They concluded that algebraic model gives better results because it introduces non-isotropic effects into calculations. In another paper, Eiamsa-ard and Promvonge [11] use the same models for numerical prediction of the processes in vortex tube, and conclude that diffusion has a great influence on maximum temperature difference achievement. In [12] and [13] a numerical study of temperature and velocity fields in the vortex tube using two-equation turbulence models within FLUENT software is conducted. Eiamsa-ard et al. [14] treated different shapes of inlet nozzles, different cold outlet dimensions and different values of the inlet pressure on the performance of the vortex tube.

Numerical analysis of the influence of cold air fraction on the values of hot and cold air temperatures is conducted in [15]. It is concluded that increase of the cooled air mass flow also increases the temperature of the heated air. The influence of the number of nozzles on the vortex tube performance is analyzed in [16], using FLUENT. The effect of length to diameter ratio was investigated in [17]. Dutta et al. [18] treat the air as real gas and obtain slightly better results in comparison to the results obtained with equation for perfect gas. They used FLUENT and standard $k-\varepsilon$ model. Parametric analysis of the vortex tube performance is considered in [19], where authors consider five different diameters of the vortex tube, use different constitutive relation for gas behavior, and different shapes and sizes of the hot outlet. Three turbulence models are used: Spalart-Almaras, $k-\varepsilon$ and Reynolds stress model, and all computations were performed using FLUENT software. It is assumed that flow in vortex tube is axisymmetric. The aim of [20] is to prove the assumption that there is optimal value of the inlet pressure for every vortex tube. Numerical calculations were conducted in FLUENT, with the use of $k-\varepsilon$ model.

In [21] the influence of the nozzles angles on the vortex tube performance is investigated, using FLUENT and $k-\varepsilon$ model. Authors also vary the inlet pressure and cold mass fraction. The main goal was to achieve the minimum cold exit temperature. The conclusion is that there is a connection between the pressure gradient along the vortex tube's axis and the cold exit temperature. Maurya and Bhavsar [22] used FLUENT and $k-\varepsilon$ model, and varied inlet pressure, orifice diameter and L/D ratio, in order to optimize the performance of the vortex tube. The effect of cold mass fraction on the movement of stagnation point and refrigeration capacity was investigated in [23], using two-equation turbulence models. In [24] artificial neural networks were used to model the effects of length to diameter ratio, the ratio of cold outlet diameter to the tube diameter, inlet pressure and cold mass fraction on the cooling performance of counter flow vortex tube. Rahbar et al. [25] numerically investigated the behavior of micro-scale vortex tubes using $k-\omega$ SST model. Khait et al. [26] investigate the energy efficiency of a double circuit vortex tube using OpenFOAM software. They vary the length of an energy separation chamber and conical angle of the hot tube, diameter of additional flow nozzle, cross section size of the main vortex nozzle as well as the degree of the additional inlet twisting. A modified version of sonicFoam solver is used, together with standard $k-\varepsilon$ model for turbulence modeling. It is shown that used mathematical model is suitable for performing of optimization computations.

In this paper, air flow in vortex tube is numerically computed using OpenFOAM – open-source CFD software. To the best of our knowledge, there are only a few references which used this software for computations of flow in vortex tube. Besides better understanding and explanations of the physics inside vortex tube, our contribution is also validation of OpenFOAM compressible solvers for computations of this kind of flow. We used two versions of software: OpenFOAM® 2.3.0 and community-driven version foam-extend 3.1. First, several implemented compressible solvers available in both versions are tested and it is found that most of the solvers give poor results. From that starting point, it was necessary to modify the codes and create two new solvers. In these new solvers energy equation is implemented in terms of total enthalpy and it is found that these solvers give physically expected results. In all computations, two turbulence models are used, $k-\varepsilon$ and $k-\omega$ SST. Similar results are obtained with both turbulence models.

Mathematical modeling and governing equations

Air flow inside vortex tube is compressible turbulent flow with highly pronounced circumferential velocity component. In addition, high temperature gradients in both axial and radial direction are present. General equations which describe the flow of any compressible medium are conservation equations of mass, momentum and energy. Written in its invariant vector form they are

$$\frac{\partial \rho}{\partial t}+\nabla\cdot\left(\rho\vec{u}\right)=0, \tag{1}$$

$$\frac{\partial\left(\rho\vec{u}\right)}{\partial t}+\nabla\cdot\left(\rho\vec{u}\otimes\vec{u}\right)=-\nabla p+\nabla\cdot\boldsymbol{T}, \tag{2}$$

$$\frac{\partial\left(\rho H\right)}{\partial t}+\nabla\cdot\left(\rho H\vec{u}\right)=\frac{\partial p}{\partial t}+\nabla\cdot\left(\vec{u}\cdot\boldsymbol{T}\right)-\nabla\cdot\vec{q}. \tag{3}$$

Additional constitutive relations are needed for closure of the system (1)-(3). We are dealing with air, which is Newtonian fluid, and it is assumed that it can be treated as calorically perfect gas. For heat flux vector $\vec{q}$ Fourier law is used. These constitutive relations are:

$$\boldsymbol{T} = \mu\left[\nabla\vec{u} + \left(\nabla\vec{u}\right)^T\right] - \frac{2}{3}\left(\nabla\cdot\vec{u}\right)\boldsymbol{I}, \quad p = \rho RT, \quad H = h + \frac{\vec{u}\cdot\vec{u}}{2}, \quad h = c_p T, \quad \vec{q} = -\lambda\nabla T. \tag{4}$$

Equations (1)-(4), together with initial and boundary conditions, theoretically enable the solution of any compressible flow of Newtonian perfect gas. But, for turbulent flows with high values of Reynolds number, like in the case of the vortex tube, direct numerical simulation of this system is followed with extremely high computational costs. Hence, turbulence modeling approach is needed in order to obtain accurate solution at acceptable computational costs. With this approach, from mathematical point of view, turbulent motion is replaced with an "equivalent flow on non-Newtonian fluid", described with additional constitutive relations. The solution of the equations used in turbulence modeling approach has more regular behavior in space and time. On the other hand, this approach lacks all of the details of real physical dynamic involved in the problem. In this work, the most common approach to turbulence modeling has been tested, namely RANS and its ability to predict energy separation process which appears in the vortex tube. In the case of a compressible flow, it is common to use Favre-averaged equations, which are given below.

Favre-averaged equations

In Favre averaging, instantaneous value of variable f is decomposed as $f = \tilde{f} + f''$, where $\tilde{f}$ is Favre averaged variable and f'' is the fluctuating part. Favre averaged variable is defined as $\overline{\rho}\tilde{f} = \overline{\rho f}$, where $\overline{(\ldots)}$ designates Reynolds averaging. In Reynolds averaging variable f is decomposed as $f = \overline{f} + f'$, where f' is the fluctuating part in respect to the Reynolds averaged value. Using Favre averaging, density fluctuations are eliminated from the averaged equations, but it does not remove the effects of density fluctuations on the turbulence, [27]. Performing Favre-averaging operations on eqs. (1)-(4), we get Favre averaged mean conservation equations in the following form:

$$\frac{\partial\overline{\rho}}{\partial t} + \nabla\cdot\left(\overline{\rho}\tilde{\vec{u}}\right) = 0, \tag{5}$$

$$\frac{\partial\left(\overline{\rho}\tilde{\vec{u}}\right)}{\partial t} + \nabla\cdot\left(\overline{\rho}\tilde{\vec{u}}\otimes\tilde{\vec{u}}\right) = -\nabla\overline{p} + \nabla\cdot\left(\overline{\boldsymbol{T}} - \overline{\rho\vec{u''}\otimes\vec{u''}}\right), \tag{6}$$

$$\begin{aligned}\frac{\partial\left(\overline{\rho}\tilde{H}\right)}{\partial t} + \nabla\cdot\left(\overline{\rho}\tilde{H}\tilde{\vec{u}}\right) = \frac{\partial\overline{p}}{\partial t} + \nabla\cdot\left[-\overline{\rho\vec{u''}h''} + \overline{\boldsymbol{T}\cdot\vec{u''}} - \overline{\rho\vec{u''}\frac{1}{2}\vec{u''}\cdot\vec{u''}}\right] \\ +\nabla\cdot\left[\tilde{\vec{u}}\cdot\left(\overline{\boldsymbol{T}} - \overline{\rho\vec{u''}\otimes\vec{u''}}\right)\right] - \nabla\cdot\tilde{\vec{q}}.\end{aligned} \tag{7}$$

and Favre averaged constitutive relations:

$$\overline{\boldsymbol{T}} = \mu\left\{\left[\nabla\tilde{\vec{u}} + \left(\nabla\tilde{\vec{u}}\right)^T\right] - \frac{2}{3}\left(\nabla\cdot\widetilde{\vec{u''}}\right)\boldsymbol{I}\right\} + \mu\left\{\left[\nabla\overline{\vec{u''}} + \left(\nabla\overline{\vec{u''}}\right)^T\right] - \frac{2}{3}\left(\nabla\cdot\overline{\vec{u''}}\right)\boldsymbol{I}\right\} = \boldsymbol{\tau} + \overline{\boldsymbol{\tau''}} \cong \boldsymbol{\tau}, \tag{8}$$

$$\overline{p} = \overline{\rho} R\tilde{T}, \quad \tilde{H} = \tilde{h} + \frac{\tilde{\vec{u}} \cdot \tilde{\vec{u}}}{2} + \frac{1}{2}\overline{\vec{u}'' \cdot \vec{u}''}, \quad \tilde{h} = c_p \tilde{T}, \quad \tilde{\vec{q}} = -\lambda \nabla \tilde{T}. \tag{9}$$

The dyad $-\overline{\rho \vec{u}'' \otimes \vec{u}''} \equiv \boldsymbol{R}$ which appears in the averaged equations is the Favre-averaged Reynolds stress tensor, in short turbulent stress tensor. Turbulent stress tensor is new unknown quantity in Favre equations, together with second term on the right hand side of the averaged energy equation, eq. (7). The most common approach for modeling of turbulent stress tensor is the Boussinesq approximation

$$\boldsymbol{R} = \mu_{\mathrm{T}} \left\{ \left[\nabla \tilde{\vec{u}} + \left(\nabla \tilde{\vec{u}} \right)^T \right] - \frac{2}{3} \left(\nabla \cdot \tilde{\vec{U}} \right) \boldsymbol{I} \right\} - \frac{2}{3} k \boldsymbol{I}, \tag{10}$$

where μ_{T} is turbulent viscosity, and $k = 0.5\overline{\vec{u}'' \cdot \vec{u}''} \equiv 0.5\mathrm{tr}(\boldsymbol{R})$ is turbulent kinetic energy. Aforementioned second unknown term consists from three terms, namely turbulent heat-flux vector, molecular diffusion and turbulent transport. It's assumed that turbulent heat-flux vector is proportional to the mean gradient of temperature as:

$$\vec{q}_t = \overline{\rho \vec{u}'' h''} = -\frac{\mu_{\mathrm{T}}}{\mathrm{Pr}_{\mathrm{T}}} \nabla \tilde{h}, \tag{11}$$

where Pr_{T} is turbulent Prandtl number. In most cases a constant value of Pr_{T} is used. In all computations in this work a constant value of 1.0 has been used, which is a default value for turbulent models used in this paper. Common expression for molecular diffusion and turbulent transport modeling is:

$$\overline{\boldsymbol{T} \cdot \vec{u}''} - \overline{\rho \vec{u}'' \frac{1}{2} \vec{u}'' \cdot \vec{u}''} = \left(\mu + \frac{\mu_{\mathrm{T}}}{\sigma_k} \right) \nabla k, \tag{12}$$

where σ_k is constant. Its value is dependent on specified model used for determination of turbulent viscosity μ_{T}. In this paper standard $k-\varepsilon$ model and $k-\omega$ SST model are used for determination of turbulent viscosity. More details about these turbulence models can be found in [28] and [29].

Compressible solvers in OpenFOAM

OpenFOAM is essentially a big set of C++ libraries intended for numerical computations in continuum mechanics. Numerical methods implemented in OpenFOAM are based on the finite volume method. The fact that OpenFOAM is written in C++ has a big advantage over CFD codes written in procedural programming languages like FORTRAN and C. Object oriented approach in programming involves abstraction, inheritance and polymorphism. That enables implementation of complicated mathematical and physical models in the code to be similar to high-level mathematical expressions, [30]. At the top level of OpenFOAM code are solvers designed for solving a specific problem in fluid mechanics. There are several compressible solvers available in OpenFOAM software. Depending of the numerical approach in solving continuity, momentum and energy equations, there are density-based and pressure-based solvers. While the pressure-based approach has been mostly used for incompressible and mildly compressible flows, the density-based approach was originally designed for high-velocity compressible flows. Both approaches are now applicable to a

broad range of flows (from incompressible to highly compressible), but density-based solvers are more accurate than the pressure-based solvers for high-speed compressible flows. Two versions of OpenFOAM software have been used for computations presented in this paper. They are OpenFOAM 2.3.0 (OF230) and community-driven version foam-extend 3.1 (fe31), while the solvers which have been used are: sonicFoam, rhoSimpleFoam, rhoPimpleFoam (from OF230) and steadyCompressibleFoam, rhoCentralFoam (from fe31).

In compressible solvers in OF230, energy equation is generally implemented in the form of total energy (enthalpy), without mechanical source term, i.e. work per unit time of viscous forces and turbulent stresses. On the other hand, in solver named steadyCompressibleFoam available in fe31 (not in OF230) mechanical source is present in the form of dissipation function, but energy equation is implemented in terms of static enthalpy. It was shown in previous researches that usage of energy equation in the form of total energy is better for prediction of energy separation phenomenon. Our initial computations with original steadyCompressibleFoam solver showed that it fails to predict energy separation phenomenon in the vortex tube. Due to its robustness and stability, the decision was made to use this solver as a base for solver in which energy equation will be implemented in terms of total enthalpy, as given by eq. (9). In energy equation, mean kinetic energy and turbulent kinetic energy are treated explicitly, based on previous calculations of velocity field from momentum equation and modeled equation for kinetic energy of turbulence. We named the new compiled solvers as steadyCompressibleTEFoam and kSteadyCompressibleTEFoam. In the first solver, kinetic energy of turbulence is neglected in comparison to two other terms in the definition of total enthalpy, eq. (9), while in the second one it was taken into account. Numerical procedure in both solvers is the same, as follows. Outer loop starts with initial assumption of the density field, then momentum and energy equations are solved for velocity and enthalpy field. Computed values of the velocity field at this stage do not satisfy continuity equation. Correction of the velocity field and determination of the pressure field is achieved with pressure-correction procedure called PIMPLE algorithm, which is a combination of SIMPLE and PISO algorithms [31], [32]. Using the corrected pressure from the last PIMPLE loop, density is updated using the equation of state.

Another solver which deserves special attention is rhoCentralFoam solver, available in both aforementioned versions of OpenFOAM. However, in fe31 original rhoCentralFoam solver does not have the ability to take into account turbulence model, so we add that ability and compile it as a new solver rhoCentralTurbFoam. This solver is density-based solver, and it solves conservation equation for unknown quantities ρ, $(\rho\vec{U})$, $(\rho\vec{E})$, where E is specific total energy. In other words, this solver use the energy conservation equation in the form where transport variable is specific total energy, i.e. the equation

$$\frac{\partial(\rho E)}{\partial t}+\nabla\cdot\left[(\rho E+p)\vec{u}\right]=\nabla\cdot(\vec{u}\cdot\boldsymbol{T})-\nabla\cdot\vec{q}, \tag{13}$$

which is basically the same equation as eq. (3), having in mind that $\rho H=\rho E+p$, by definition of enthalpy. First step in numerical algorithm of this solver is the calculation of density field from continuity equation. Then momentum equation without diffusion terms is solved for intermediate estimation of momentum $(\rho\vec{U})$. After this step, momentum equation with diffusion terms included is solved for velocity field $\vec{U}$ and field $(\rho\vec{U})$ is updated. Then, energy equation is solved for (ρE), excluding the heat flux term. Using solutions for (ρE) and $\vec{U}$ fields, intermediate value of specific internal energy e is calculated. Equation for e is

then solved including the heat flux term. At the end of the loop, values of e, (ρE) are updated, and the pressure field is calculated from the equation of state.

Test geometry and case set-up

Simplified axisymmetric geometry of the vortex tube considered in this paper is shown in fig. 1. Corresponding dimensions are: $L = 520\,\text{mm}$, $L_c = 130\,\text{mm}$, $r = 47\,\text{mm}$, $r_c = 17.5\,\text{mm}$ and diameters of inlet, hot and cold outlets are equal to $d = 16.25\,\text{mm}$. Experimental investigation of the flow in this vortex tube was performed by Bruun [33]. Previous numerical studies on the same geometry were performed by Fröhlingsdorf and Unger [6], and we use this case as our first test case for computations of the flow in a vortex tube. For mesh generation block structured mesh generator blockMesh available within OpenFOAM has been used. In standard $k-\varepsilon$ model wall functions are used to bridge the viscous sublayer, so during mesh generation process, care is taken that the y^+ value is approximately equal to 30 near all walls (this value is confirmed later during computations). Also, the grading is introduced in areas in which high gradients of physical quantities are expected. The boundary conditions are set as follows. At the inlet, values of velocity and temperature are set to $\vec{U} = -19.4\vec{j} + 199\vec{k}\,[\text{m/s}]$ and $T = 274.3\,\text{K}$, while for the pressure Von Neumann zero gradient condition is used. For turbulence quantities (k, ε or ω) it is assumed that turbulence intensity is 5% of the mean velocity, and that integral length scale is 10% of the inlet dimension. The boundary condition for velocity, temperature and turbulence quantities on the outlets is the so called inletOutlet boundary condition. It allows the possibility of reverse flow, i.e. it switches between fixed value and zero gradient condition, dependent on the direction of the velocity vector. Fixed values of pressure are prescribed on outlets: 1.013 bar at cold outlet and 1.138 bar at hot outlet. At walls, no-slip condition is used for velocity, zero gradients for pressure and temperature and wall functions for turbulence quantities.

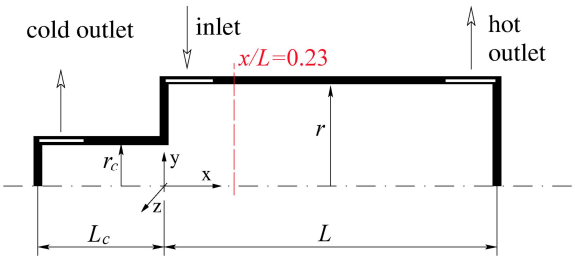

Figure 1. Geometry of the vortex tube, [6].

Even though the problem is essentially considered as steady, we used transient terms in some solvers. Usage of this term enhanced stability of the solvers, with steady solution achieved at the end of computations. For this term we used Crank-Nicolson 0.5 discretization scheme with adjustable time step. It is a combination of fully implicit and fully explicit methods, so it evaluates the values of the dependent variables at both the old and new time levels. For steady state solvers, we used under-relaxation procedure to assure the convergence of the solution. Discretization of the convection term in momentum equation is performed by Total Variation Diminishing (TVD) scheme. An improved version of the limited scheme is applied for the velocity field, in which the limiter is formulated to take into account the direction of the field. In the solver rhoCentralFoam convection term is discretized with the second order semi-discrete flux-splitting scheme of Kurganov and Tadmor [34]. More information about implementation of this scheme in rhoCentralFoam solver can be found in [35]. Second order upwind (linearUpwind) scheme is used for discretization of convective terms in equations for turbulence quantities. Diffusion term is discretized using unbounded, second order, conservative scheme. The tolerance for matrix solvers for pressure field is set to

10^{-8}, while for the velocity and density field, as also for turbulence fields it is set to 10^{-5}. Relative tolerance is set to 0 which forced the solution to converge to the imposed tolerance in each time step. Concerning the physical properties, we treated the air as a perfect gas, with constant values of viscosity $\mu = 1.8 \cdot 10^{-5}$ N/(m²s) and laminar Prantdl number $\mathrm{Pr} = 0.7$.

Results and discussion

Mesh and solution convergence analysis

For mesh convergence analysis three meshes with 26500 (M1), 31500 (M2) and 36040 (M3) cells are used. By monitoring and comparing the obtained results for fields of physical quantities for these meshes it is observed that results on M2 and M3 practically coincide and that desired accuracy is reached, with lower computational costs. The temperature profiles at cross-section $x/L = 0.23$ for meshes M1, M2 and M3 are shown in fig. 2, using steadyCompressibleTEFoam solver. Similar behavior concerning mesh independence analysis is noticed with all other solvers. So, mesh M2 is used in all computations presented in the following sections.

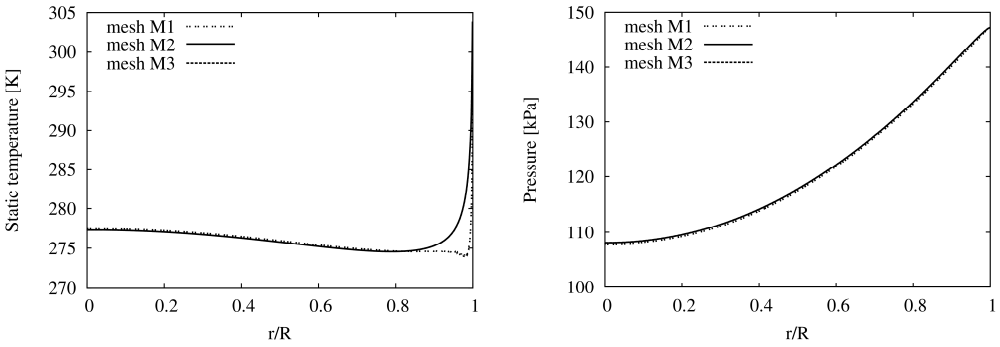

Figure 2. Mesh independence test results in cross section $x/L = 0.23$ with the use of steadyCompressibleTEFoam, $k-\varepsilon$ model.

Solution convergence is checked by monitoring the residuals, but also the changes of physical quantities inside the flow domain during computations. What is common for all tested solvers is relatively high computational time for obtaining the steady state solution. For example, starting from initial, homogeneous distribution of physical quantities inside the domain, it took 18 hours and 10 minutes on Intel R Core (TM) i7-2600K 8CPU @ 3.40GHz to obtain fully convergent, steady-state solution using solver steadyCompressibleTEFoam on mesh M2 (400000 outer iterations). Changes of temperature and pressure during computations for that case, in two points inside computational domain are shown in fig. 3.

It is noticeable that convergence of pressure field is reached earlier than convergence of temperature field. Computational time is slightly decreased using mapping procedure, i.e. interpolating the final results obtained on mesh M1 to initial values of physical quantities on mesh M2.

As mentioned before, main goal of this research is to test various compressible solvers available in OpenFOAM for computations of the flow in a vortex tube. Information about the solvers which are used is given in the previous section. Using solver

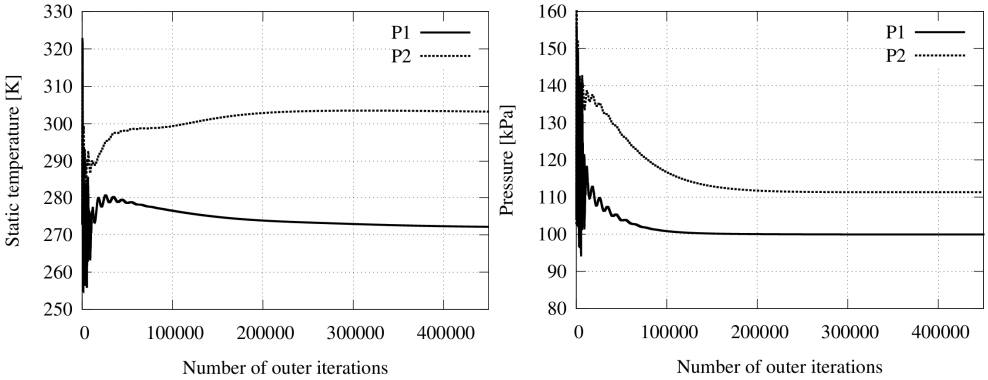

Figure 3. Changes of temperature and pressure during iteration procedure. Solver steadyCompressibleTEFoam, mesh M2, $k-\varepsilon$ turbulence model. Point coordinates: P1$(0.01,0.001,0)$, P2$(0.3,0.001,0)$.

rhoSimpleFoam, a converged steady state solution is not achieved and high oscillations in residual values are noticed. Temperature field also exhibits oscillatory behavior after some (large) number of outer iterations. Similar behavior is also noticed during simulations with steadyCompressibleFoam and $k-\omega$ SST model. Solver sonicFoam is used in transient mode, with fixed value of the time step: $\Delta t = 5\cdot 10^{-7}$ s. This value insured the initial value of Courant number is lower than 0.5. In other transient solvers we used adjustable time step, with criteria that the value of Courant number is always lower than 0.3. Adjustable time step enables lower computational time. In the case of rhoCentralTurbFoam simulations, averaged value of time step has the order of 10^{-8} s. Although converged, steady-state solution obtained with rhoPimpleFoam solver, i.e. corresponding temperature field obtained using $k-\omega$ SST is completely unphysical. With $k-\varepsilon$ model and the same solver, we have more physical distribution to some extent, but not on the satisfactory level.

Temperature and velocity field

Results of all solvers with converged steady-state solution are given in tab. 1.

Table 1. Average values of air total temperature at the outlets of the vortex tube (Total temperature at the inlet is equal to 294.2 K); ncs – non-convergent solution.

SOLVER	TOTAL TEMPERATURE [K]					
	$k-\varepsilon$ model		$k-\omega$ SST model		Experiment	
	cold	hot	cold	hot	cold	hot
sonicFoam	285.2	296.2	311.7	336.5	274	300
rhoPimpeFoam	287.3	304.4	281.5	222.7		
steadyCompressibleFoam	324.5	401.7	ncs	ncs		
steadyCompressibleTEFoam	275.9	303.5	276.8	303.1		
kSteadyCompressibleTEFoam	276.1	303.4	277.5	302.4		
rhoCentralTurbFoam	273.8	301.1	274.3	300.4		

It is evident that energy separation phenomenon is captured with steadyCompressibleTEFoam, kSteadyCompressibleTEFoam and rhoCentralTurbFoam solvers. Comparison of the results of outlet temperatures obtained with the first two solvers

shows that neglecting the k in the definition of total enthalpy in Favre averaged equations is completely justified in this case. At the same time, both solvers predict the same distributions of total temperature inside computational domain. Detailed analysis has shown this is also the case with the static temperature distribution, as well as with all other physical quantities computed.

The best agreement with experimental values of total temperature at outlets of vortex tube is obtained with rhoCentralTubeFoam and $k-\omega$ SST turbulent model. But, in general it can be stated that both turbulent models and all three solvers give very good prediction of total temperature values at cold and hot outlet of vortex tube. In that sense, results of steadyCompressibleFoam and rhoCentralTurbFoam will be further presented and compared.

First, we compare the radial distributions of static and total temperature, shown in fig. 4. Diagrams show some differences in temperature distribution. Solver rhoCentralTurbFoam predicts lower values of both static and total temperature in nearly whole cross-section. This temperature difference is also present in the values of temperatures at hot and cold outlet of vortex tube. The biggest difference between the results of temperature distribution is near the pipe wall, where steadyCompressibleTEFoam predicts higher temperature gradients, and maximum of total temperature practically at the pipe wall, while rhoCentralTurbFoam predicts the maximum at dimensionless distance $r/R=0.993$. Other authors also report that total temperature maximum is not at the pipe wall as well as high temperature gradients at the wall, for example [12], [23], [36]. Comparison with experimental results in the cross-section $x/L=0.23$ for total temperature shows quite good agreement with experimental results, as it is shown in fig. 4. Similar distributions of temperature, with their slightly lower values for both solvers are obtained with $k-\omega$ SST model.

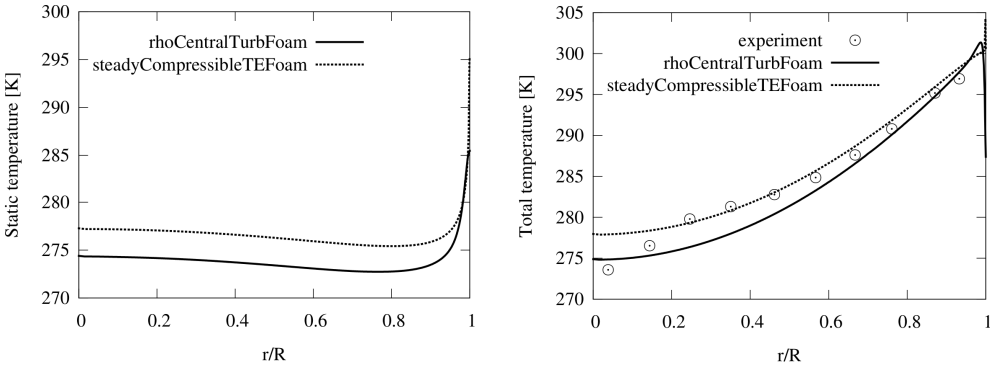

Figure 4. Temperature profiles in cross section $x/L=0.23$ obtained using $k-\varepsilon$ model with solvers steadyCompressibleTEFoam and rhoCentralTurbFoam.

What is to note is that these two solvers using the same turbulent model give slightly different results of temperature field, which is also the case for other physical quantities. This is normal since they have different numerical procedures implemented, as explained earlier. Solver steadyCompressibleTEFoam proved to be more robust for calculations, while on other hand rhoCentralTurbFoam gives results which are in slightly better agreement with experimental data. What we found as the most convenient procedure for computations is to

first make calculations with steadyCompressibleTEFoam, and then use its final results as the starting data for computations with rhoCentralTurbFoam solver.

Now, we present the differences in results of velocity field obtained with the same solver, but with different turbulent models. Figure 5 shows profiles of axial and

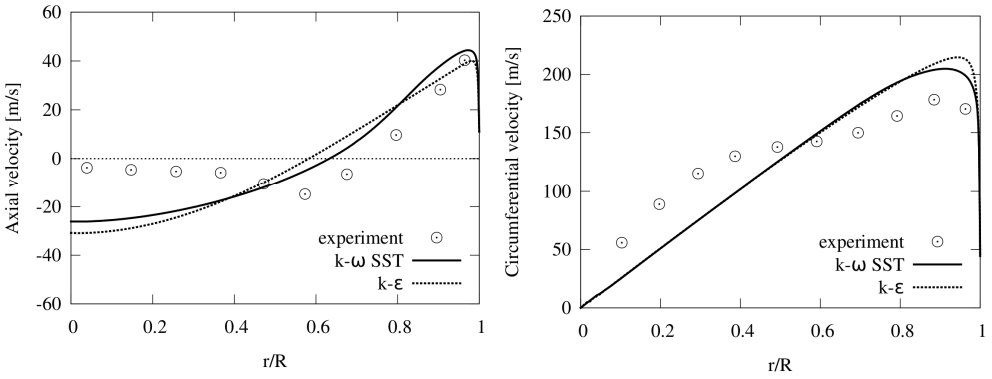

Figure 5. Circumferential and axial velocity profiles in cross-section $x/L = 0.23$ obtained using $k-\varepsilon$ and $k-\omega$ SST model with solver rhoCentralTurbFoam.

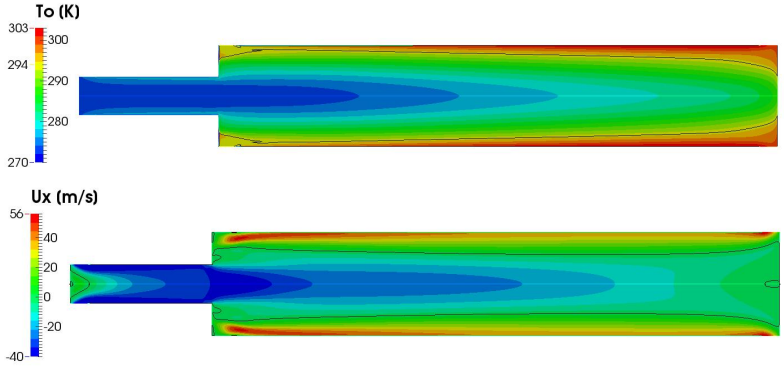

Figure 6. Total temperature and axial velocity contours – black lines designates contour $T_0 = 294\,\mathrm{K}$ (value of inlet total temperature) and $U_x = 0\,\mathrm{m/s}$; solver rhoCentralTurbFoam, $k-\omega$ SST model.

circumferential velocity components in the cross-section $x/L = 0.23$, obtained with rhoCentralTurbFoam solver and $k-\varepsilon$ and $k-\omega$ SST turbulent models. Experimental data are also shown in the same figure. What is obvious is that both turbulent models fail to predict the velocity field in a good manner. Slightly better agreement is obtained with $k-\omega$ SST model. What is common for both models is that they overpredict the value of axial velocity component in the backflow region around the pipe axis, while underpredict the circumferential velocity component in the same region. This is a well-known weakness of all turbulent models based on linear, scalar eddy viscosity assumption given by eq. (10) in prediction of highly swirling flows, [37]. All models based on this assumption predict the so-called ”solid-body” profile for circumferential velocity component, for which in the large part of the pipe cross-section fluid rotates around the pipe axis with constant angular velocity. In

most cases of the vortex tube design circumferential velocity component should have approximately this type of profile, due to the fact that the air is injected in the pipe tangentially through the nozzles located close the pipe wall. However, due to complex physics inside the vortex tube, some level of discrepancy from the ”solid-body” profile can be expected, which experimental data clearly shows. On the other hand, in Bruun’s experiments, mean velocities are not directly measured, but calculated from measurements of total pressure and total temperature using very simplified forms of conservation equations. It is obvious that it’s necessary to test the solvers on some other geometries of the vortex tube, to make a stronger validation. Also, our current and future work is devoted to computations using full Reynolds stress closure models. This type of models is better suited for computations of highly swirling flows [37], [38], but they exhibit more problems with solution convergence. In our initial computations, we could not get a converged solution for the test case considered.

Finally, fig. 6 shows the contours of total temperature and axial velocity component inside the vortex tube, obtained with $k-\omega$ SST turbulent model. For better representation, computational domain is mirrored around *x*-axis. Distribution of total temperature clearly shows energy separation phenomenon, where region of hotter air is near the pipe wall in which the air flows in the positive *x*-direction, while colder air is grouped around the pipe axis and it flows in the negative *x*-direction, towards the cold outlet.

Conclusions

Compressible flow of air inside Ranque-Hilsch vortex tube is numerically investigated using OpenFOAM, open source CFD software. OpenFOAM has proved as a reliable tool for computations of incompressible flows, while for compressible flows there is a need for more comprehensive validation. Our investigation shows that almost every compressible solver available in OpenFOAM fails to predict the typical flow characteristics of the flow inside vortex tube. However, due to benefits of open-source philosophy, it was possible to study and understand how compressible solvers are implemented in the OpenFOAM code. In that spirit, the code of steadyCompressibleTEFoam solver is modified and energy equation was written in the form of total energy conservation, instead of original conservation equation for thermal energy. This modification proved as the key factor for prediction of temperature separation phenomenon in the appropriate manner. On the other hand, rhoCentralFoam solver in its original implementation (with slight modification of the code in fe31 version, as explained in the paper) also predicts physically expected temperature stratification. Results of these two solvers have some slight differences, which is a consequence of different numerical procedures implemented in their codes. Solver steadyCompressibleTEFoam shows as more robust. Comparison with experimental data showed good agreement, especially for temperature distribution. Velocity distribution is not predicted in a good manner, due to the fact that turbulent models based on linear, scalar eddy viscosity assumption are used. In most cases, this is inappropriate assumption for modeling highly swirling flows, which is shown in previous researches. Current and future work is dedicated to computations of flow in a vortex tube with full Reynolds stress closure models, using solvers presented in this paper.

Acknowledgment

The authors of this paper gratefully acknowledge financial support provided by the Ministry of Education, Science and Technological Development, Republic of Serbia (Project No. TR 35046).

Nomenclature

H - mean total enthalpy per unit mass, [J/kg]
$\boldsymbol{R}$ - Reynolds stress tensor, [kg/(ms^2)]
$\boldsymbol{T}$ - viscous stress tensor, [Pa]
T - temperature, [K]
T_0 - total temperature, [K]
$\vec{u}$ - velocity vector, [m/s]

Greek symbols

ε - energy dissipation rate, [m^2/s^3]
λ - thermal conductivity, [W/(mK)]
μ - viscosity, [Pas]
ρ - density, [kg/m^3]
$\boldsymbol{\tau}$ - mean viscous stress tensor, [Pa]
ω - specific dissipation rate, [1/s]

References

[1] Ranque, G., Experiences sur la detente giratoire avec simultanes d'un echappement dair chaud et dun enchappement d'air froid, *J. Phys. Radium, 4* (1933), 7, pp. 112–114
[2] Hilsch, R., The use of the expansion of gases in a centrifugal field as cooling process, *Rev. Sci. Instrum, 18* (1947), 2, pp. 108–113
[3] Kurosaka, M., Acoustic streaming in swirl flow and the Ranque-Hilsch (vortex-tube) effect, *Journal of Fluid Mechanics, 124* (1982), pp. 139–172
[4] Ahlborn, B., Groves, S. Secondary flow in a vortex tube, *Fluid Dyn. Res 21* (1997), pp. 73–86
[5] Ahlborn, B, Gordon, J., The vortex tube as a classic thermodynamic refrigeration cycle, *J. Appl. Phys., 6* (2000). pp. 36453653
[6] Fröhlingsdorf, W., Unger H., Numerical investigations of the compressible flow and the energy¨ separation in the Ranque-Hilsch vortex tube, *International Journal of heat and mass transfer, 42* (1999) pp. 415–422
[7] Aljuwayhel, F., *et al.*, Parametric and internal study of the vortex tube using a CFD model, *International Journal of Refrigeration 28* (2005), pp. 442–450
[8] Skye, H.M., *et al*, Comparison of CFD analysis to empirical data in a commercial vortex tube, *International Journal of Refrigeration 29* (2006), pp. 71–80
[9] Behera. U., *et al.*, CFD analysis and experimental investigation towards optimizing the parameters of Ranque-Hilsch vortex tube, *International journal of heat and mass transfer 48* (2005), pp. 1961–1973
[10] Eiamsa-ard, S., Promvonge, P. Numerical prediction of vortex flow and thermal separation in subsonic vortex tube, *Journal of Zhejiang University SCIENCE A 7* (2012), 8, pp. 1406–1415
[11] Eiamsa-ard, S., Promvonge, P., Numerical investigation of the thermal separation in a RanqueHilsch vortex tube, *International Journal of Heat and Mass Transfer 50* (2007), pp. 821–832
[12] Behera, U., *et al.*, Numerical investigations on flow behaviour and energy separation in RanqueHilsch vortex tube, *International journal of heat and mass transfer 51* (2008), pp. 6077–6089
[13] Secchiaroli, A., *et al.*, Numerical simulation of turbulent flow in a Ranque-Hilsch vortex tube, *International Journal of Heat and Mass Transfer 52* (2009), pp. 5496–5511
[14] Eiamsa-ard, S., *et al.*, Experimental investigation on energy separation in a counter-flow RanqueHilsch vortex tube: Effect of cooling a hot tube, *Int. Comm. Heat Mass Transfer vol. 37* (2010), pp. 156–162
[15] Pourmahmoud N., Akhesmeh, S., Numerical investigation of the thermal separation in a vortex tube, *World Academy of Science, Engineering and Technology 43* (2008), pp. 399–405
[16] Shamsoddini, R., Nezhad, A. H., Numerical analysis of the effect of nozzles number on the flow and power of cooling of a vortex tube, *International Journal of Refrigeration 33* (2010), pp. 774–782
[17] Bramo, A. R., Pourmahmoud, N., Computational fluid dynamics simulation of length to diameter ratio effects on the energy separation in a vortex tube, *Thermal Science, 15* (2011), 3, pp. 833–48

[18] Dutta, T., *et al.*, Numerical investigation of gas species and energy separation in the Ranque-Hilsch vortex tube using real gas model, *International Journal of Refrigeration 34* (2011), pp. 2118–2128
[19] Khazei, H., *et al.*, Effects of gas properties and geometrical parameters on performance of a vortex tube, *Scientia Iranica, Transactions B: Mechanical Engineering 19* (2012), 3, pp. 454–462
[20] Pourmahmoud, N., *et al.*, Numerical investigation of operating pressure effects on performance of a vortex tube, *Thermal Science 16*, (2012), 1, pp. 151–66
[21] Pourmahmoud, N. *et al.*, Optimization of low pressure vortex tube via different axial angles of injection nozzles, *International Journal of Engineering 26* (2013), 10, pp. 1255–1266
[22] Maurya, R. S., Bhavsar, K. Y., Energy and flow separation in the vortex tube: A numerical investigation, *International Journal on Theoretical and Applied Research in Mechanical Engineering (IJTARME), 2* (2013), 3, pp. 2319–3182
[23] Pouraria, H. and Park, W., Numerical investigation on cooling performance of Ranque-Hilsch vortex tube, *Thermal Science, 18* (2014), 4, pp. 1173–89
[24] Pouraria, H., *et al.*, Modeling the cooling performance of vortex tube using a genetic algorithm – based artificial neural network, *Thermal Science, 20* (2016), 1, pp. 53-65.
[25] Rahbar, N., *et al.*, Numerical investigation on flow behaviour and energy separation in a micro-scale vortex tube, *Thermal Science, 19* (2015), 2, pp. 619–30
[26] Khait, A. V., *et al.*, Mathematical simulation of Ranque-Hilsch vortex tube heat and power performances, *14th International Conference on Computing in Civil and Building Engineering*, (2013), pp. 1–8
[27] D. C. Wilcox, D. C., *Turbulence modeling for CFD*. DCW Industries, Inc. La Canada, California, 2 ed., 1994.
[28] Launder, B., Sharma, B., Application of the energy dissipation model of turbulence to the calculation of flows near a spinning disk, *Letters in Heat and Mass Transfer, 1* (1974), pp. 131–138
[29] Menter, F. R., Two-equation eddy-viscosity turbulence models for engineering applications, *AIAA Journal 32* (1994), 8, pp. 1598–605
[30] Weller, H., *et al.*, A tensorial approach to cfd using object orientated techniques, *Computers in Physics 12* (1998), 6, pp. 620–631
[31] Issa, R., Solution of the implicitly discretized fluid flow equations by operator splitting, *Journal of Computational Physics 62* (1986), pp. 40–65
[32] Patankar, S., Spalding, D., A calculation procedure for heat, mass and momentum transfer in threedimensional parabolic flows, *International Journal of Heat and Mass Transfer 15* (1972), pp. 1787–1806
[33] Bruun, H. H., Experimental investigation of the energy separation in vortex tubes, *J. Mechanical Engineering Science 11* (1969), 6, pp. 567–582
[34] Kurganov, A., Tadmor, E., New high-resolution central schemes for nonlinear conservation laws and convection-diffusion equations, *Journal of Computational Physics 160* (2001), pp. 241–282
[35] Greenshields, C. *et al.*, Implementation of semi-discrete, non-staggered central schemes in a colocated, polyhedral, finite volume framework, for high-speed viscous flows, *International Journal for Numerical Methods in Fluids 63* (2010), 1, pp. 1–21
[36] Farouk T., Farouk, B., Large eddy simulations of the flow field and temperature separation in the Ranque-Hilsch vortex tube, *International Journal of Heat and Mass Transfer 50* (2007), pp. 4724–4735
[37] Jakirlić, S., *et al.*, Modeling rotating and swirling turbulent flows: a perpetual challenge, *AIAA Journal 40* (2002), 10, pp. 1984–1996
[38] Ćoćić, A., *et al.*, Numerical analysis of axisymmetric turbulent swirling flow in circular pipe, *Thermal Science 18* (2014), 2, pp. 493–505

Paper submitted: February 23, 2016
Paper revised: May 17, 2016
Paper accepted: June 19, 2016